Study of Droplet Sprays Prior to Impact on a Heated Horizontal Surface

J. E. González
ASME Assoc. Mem.
Assistant Professor
jo_gonzalez@rumac.upr.clu.edu
Department of Mechanical Engineering,
University of Puerto Rico-Mayagüez,
Mayagüez, Puerto Rico 00680

W. Z. Black
Regents Professor
ASME Fellow
George W. Woodruff School
of Mechanical Engineering,
Georgia Institute of Technology,
Atlanta, GA 30332

This paper concerns a quantitative assessment of the heat and mass transfer behavior of spray droplets, downward oriented prior to their impact on a heated horizontal surface. An experimental and theoretical investigation of the coupling effects between a downward oriented spray and a rising saturated buoyant jet that results from evaporation of the spray on a heated surface has been successfully completed. A model describing the coupled thermal and hydrodynamic behavior of both the spray and the saturated buoyant jet has been developed. An experimental set-up involving a high speed photographic apparatus has been used to observe in-flight monodispersed sprays and to measure the diameter and the velocity of droplets as they approach the heated surface. The theoretical and experimental results indicate that the temperature of the saturated buoyant jet is highly affected by the presence of a subcooled spray and small droplet sprays, vertically projected, experience high condensation rates as they pass through the saturated buoyant jet, reaching the saturation temperature before impacting on the heated surface, as well as experience acceleration as a consequence of an increase in mass due to the condensation.

Introduction

During recent years there has been an increased demand for new techniques capable of removing high heat fluxes and it is expected that this demand will continue to increase in the future. The most commonly used cooling technologies utilize natural and forced single-phase convection mechanisms, while natural and forced two-phase convection and microchannel cooling appear to be the types of techniques used to cool devices which generate high heat fluxes such as in microelectronics and fusion components.

Pool boiling can be achieved by submerging a hot surface in a stagnant liquid column or by injecting the working fluid directly on the surface. For situations which involve a surface temperature close to the saturation temperature of the liquid, the second method is more desirable because of the reduction of the excess liquid. The injection of the liquid can be achieved by using a continuous, single phase jet or by using a mixture of a discrete and a continuous phase. The first case is known as jet impingement cooling and the second one as spray cooling. Researchers (Bonacina et al., 1979; Choi and Yao, 1987; Ghodbane and Hollman, 1991; Pedersen, 1970; Toda, 1974) have shown that heat fluxes in excess of 100 W/cm^2 can be obtained with either technique. Gu et al. (1993) reported spray cooling heat fluxes 50 percent higher than single-phase impingement jet. This increase in heat flux is attributed to the control of uniform thin liquid films that can be obtained with spray cooling.

Because of its potential to remove high heat fluxes, spray cooling has found applications in a wide range of industrial processes including (1) the nuclear industry, to cool the fusion components (Watson, 1990); (2) the medical industry, to cool ion beam targets (Bacon et al., 1984); (3) the metallurgical industry, to achieve fast and control cooling (Hall and Mudawar, 1995); and (4) the ceramic industry, for thermal tempering (Ohkubo and Nishio, 1987).

Contributed by the Heat Transfer Division for publication in the JOURNAL OF HEAT TRANSFER. Manuscript received by the Heat Transfer Division February 6, 1996; revision received November 14, 1996; Keywords: Boiling, Modelling & Scaling, Sprays/Droplets. Associate Technical Editor: B. Webb.

The general study of a liquid spray propelled toward a heated surface can be divided into two subprocesses: the behavior of the droplets prior to impacting on the heated surface, and the dynamics of the drops after they hit the surface. The post-impact process is characterized by the spreading and evaporation of the liquid droplets. On the other hand the pre-impact process is characterized by the bulk convective heat and mass transfer that occur between the spray and surroundings before the drops impact the surface. The majority of the experimental and theoretical works have concentrated on the post-impact spray phenomenon and little effort has gone to studying the pre-impact problem even though the pre-impact behavior will have significance in the overall heat transfer process. The importance of pre-impact effects was first reported by Choi and Yao (1987) and Deb and Yao (1989) in film boiling experiments.

This research investigates the thermal behavior of vertical downward-directed small droplet sprays before they impact on a hot horizontal surface under nucleate boiling condition, and it attempts to fill a void in the full understanding of the spray cooling phenomena. The pre-impact spray cooling problem involves the solution of two coupled sub-problems, namely: (1) evaluation of the thermal behavior of a spray as it approaches the surface after having traveled through a medium with variable thermal and transport properties, and (2) evaluation of the thermodynamic and hydrodynamic states of a mixture of water vapor and air surrounding the surface. The latter includes evaporation from the surface as well as the possibility of both evaporation and condensation in the spray.

The general problem of heat and mass transfer between a gas phase and a discrete liquid phase has been addressed in the combustion gases literature (see for example Zhou, 1993; Liu and Reitz, 1995). However, in spray cooling applications, a mixed convective nonreacting binary gas may result from liquid evaporation at the heated surface that will dynamically and thermally interact with a downward projected spray, making this the problem unique. The primary focus of this paper is to look into the details of this particular coupled problem.

To insure validity of the analysis, the results were compared with measurements made in experiments designed to simulate the behavior of small-droplet sprays projected toward a heated surface. The variables observed in the experiments are the drop-

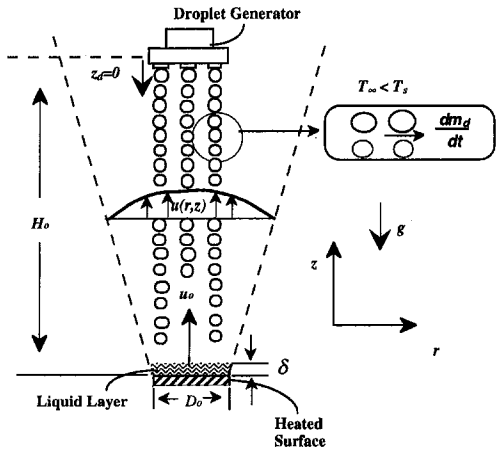

Fig. 1 Schematic of the general problem

let diameters and velocities, as a function of the vertical position. The range of spray properties was limited to nucleate boiling conditions. A monodispersed spray of liquid water at one atmosphere pressure was chosen as the working fluid for these experiments.

Mathematical Formulation

Figure 1 shows a spray of liquid droplets approaching a heated surface. The temperature of the heated plate is high enough to cause evaporation of a liquid film on the surface. The vapor coming from the liquid film will rise and diffuse into the surroundings due to a combination of inertia and buoyancy effects. The thermodynamic state of the resulting buoyant jet will have a strong influence on the temperature and velocity of the droplets as they pass through the gas.

Furthermore, the thermodynamics and physical state of the drops depend upon whether they experience evaporation or condensation with the ambient vapor. Evaporation from the droplets will also have an effect on the buoyant jet due to the heat transfer and mass addition that results from the droplets. Condensation of the vapor may occur on the liquid drops if the partial pressure of the vapor in the buoyant jet is higher than the saturation pressure evaluated at the liquid drop temperature. If the initial temperature of the droplets is lower than the local saturation temperature of the binary gas, the droplets will also experience a sensible heating from the warm jet. Condensation of the vapor in small aerosols, normally present in the ambient, may also occur. The thermal models of the drops and the plume must consider all these factors.

Single Drop Thermal Model. The analysis considers a single drop and utilizes a Lagrangian viewpoint following a single droplet from its injection into the ambient vapor until it approaches the heated surface. Droplets are assumed to be small enough so as to remain spherical with uniform thermal properties. Other assumptions are as follows:

- vapor flow around a drop surface is assumed to be quasi-steady
- vapor and liquid phases are in thermodynamic equilibrium
- the drops do not collide
- radiation heat transfer from the drops is negligible
- buoyancy effects are negligible
- potential and kinetic energy changes of a droplet are small
- the drop moves in a two-dimensional Cartesian space

With these assumptions in mind, the equations for conservation of energy, momentum, and mass of a single droplet are written as a function of time. This is achieved by considering that the thermal state of the droplet is a function of the z and r directions by considering drag, gravity, and Saffman forces and by using a Lagrangian viewpoint so that the control volume always surrounds the moving droplet. The conservation equations then become:

Nomenclature

C_d = drag coefficient
c_p = specific heat
D = diameter of a droplet
D_{ab} = diffusivity of water vapor in air
D_o = heater plate diameter
f = frequency
G = mass flow rate
Gr = Grashoff number = $g(T_o - T_\infty)H_o^3/(\bar{T}\nu^2)$
g = acceleration of gravity
H_o = height between drop generator and heated plate
h = heat transfer coefficient for liquid droplets
h_{fg} = latent heat of vaporization of water
h_m = mass transfer coefficient for liquid droplets
k = thermal conductivity, condensation/evaporation rate
L = spacing between droplets
M = molecular weight
m = mass of single droplet or condensing particle
N_o = density number
p = total pressure
p_a = mean local gas partial pressure between the droplet surface and the buoyant jet
q'' = heat flux
Re = Reynolds number of the droplet = Du_d/ν
Re_H = Reynolds number of the buoyant jet = $H_o u_o/\nu$
r = radial direction
r_c = local radius of the condensation particles
Sc = Schmidt number = ν/D_{ab}
T = temperature
t = time
u = velocity component in the axial direction
v = velocity component in the radial direction
X_A = mass fraction of water vapor = ρ_A/ρ
Z = nondimensional axial coordinate = z/H_o
z = axial direction

Greek Symbols

α = thermal diffusivity = $k/(\rho c_p)$
Δp = water vapor pressure difference at the drop surface = $p_{sd} - p_a$
ν = kinematic viscosity
μ = dynamic viscosity
ρ = total density = $\rho_A + \rho_B$
σ = surface tension
θ = $(T - T_\infty)/(T_o - T_\infty)$

Subscripts

A = water vapor
B = dry air
c = aerosol particles value
cl = value evaluated along the jet centerline
D = drag, diameter
d = droplet value
i = initial value
j = liquid jet out of the droplet generator
m = value of the mixture in the buoyant jet
l = liquid water
o = initial jet value
r = reference value for the drag coefficient
s = surface of the droplet, saturation value
sat = saturated value
v = water vapor
∞ = surroundings

Conservation of Momentum in the Axial Direction.

$$\frac{d(D^3u_d)}{dt} = (D^3g) - \left(\frac{3}{4}\right)\left(\frac{\rho_m}{\rho_l}\right)D^2C_{dz}(u_d - u)|u_d - u| \quad (1)$$

Conservation of Momentum in the Radial Direction.

$$\frac{d(D^3v_d)}{dt} = -\frac{6.46\mu(v_d - v)D^2}{4(\nu)^{1/2}\rho_l}\left(\frac{\partial u}{\partial r}\right)^{1/2} - \left(\frac{3}{4}\right)\left(\frac{\rho_m}{\rho_l}\right)D^2C_{dr}(v_d - v)|v_d - v| \quad (2)$$

Conservation of Energy.

$$\frac{dT_d}{dt} = \frac{3h_{fg}}{c_{pl}}\frac{dln(D)}{dt} - \frac{6h}{D\rho_l c_{pl}}(T_d - T(r, z)) \quad (3)$$

Conservation of Mass.

$$\frac{dD}{dt} = -2\left(\frac{M_v}{M_m}\right)\left(\frac{\rho_m}{\rho_l}\right)\left(\frac{\Delta p}{p_b}\right)\left(\frac{D_{ab}}{D}\right) \times (2.0 + 0.6\,\mathrm{Sc}^{1/3}\,\mathrm{Re}^{1/2}) \quad (4)$$

Initial Conditions.

$$u_d(0) = -u_{di}, \quad v_d(0) = 0; \quad T_d(0) = T_{di}, \quad D(0) = D_i$$

The first term in the right side of Eq. (2) refers to the Saffman force. While this force is usually small, it can be significant in viscous fluids with high velocity gradients, thus creating a force perpendicular to the velocity of the main flow (Saffman, 1965; Saffman, 1968).

Drag Coefficient of Droplets. The drag coefficient for a single evaporating or condensing sphere is obtained from Yuen and Chen (1976) as

$$C_D = C_{Do}\frac{\mu_{m\infty}}{\mu_{mr}} \quad (5)$$

where C_{do} is the drag coefficient of a solid sphere, and μ_{mr} is the viscosity of the water vapor and air mixture. The viscosity μ_m depends on the reference temperature and the reference water vapor concentration, defined by Yuen and Chen (1976) as

$$T_r = T_d + 1/3(T + T_d) \quad X_{Ar} = X_{Ad} + 1/3(X_A + X_{Ad}). \quad (6)$$

The drag coefficient of a solid sphere, C_{do}, corresponds to that of an accelerated particle which can be obtained from Fuchs (1964):

$$C_{Do} = \frac{27}{\mathrm{Re}^{0.84}}. \quad (7)$$

The droplets in this problem may travel at close spacings to each other and their drag coefficient may be affected by the wake formed by the upstream drops. Experimental evidence shows that droplets traveling at close distances from each other may have a drag coefficient that is less than the drag coefficients calculated for an isolated sphere by a factor of four and five (Mullholland, 1988; Poo and Ashgriz, 1991). Mullholland (1988) suggested a drag coefficient model which accounts for the effects of droplet interaction based on the superposition of the drag coefficient of an isolated droplet and that of a long rod:

$$C_D(\mathrm{Re}, L/D)^{-n} = [C_D^{\infty}(\mathrm{Re})]^{-n} + [C_D^0(\mathrm{Re}, L/D)]^{-n}. \quad (8)$$

In Eq. (8), $C_D^{\infty}(\mathrm{Re})$ is the drag coefficient of an evaporating droplet which is given by Eq. (5), a and n are experimental constants and

$$C_D^0(\mathrm{Re}, L/D) = C_{D\text{-rod}}(\mathrm{Re}) + \frac{a}{\mathrm{Re}}(L/D - 1). \quad (9)$$

Here $C_{D\text{-rod}}(\mathrm{Re})$ is the drag coefficient for a cylinder of diameter D. The constants a and n were experimentally determined by Mullholland (1988) to be 0.678 ± 0.07 and 43.0 ± 15.4, respectively, for a range of Reynolds numbers between 1 and 250, and a range of droplet spacing to diameter ratios, L/D, between 10 and 50. The critical value for L/D is defined as the nondimensional droplet spacing for which the droplet drag coefficient starts to be affected by the presence of adjacent droplets.

Solution to Eqs. (1) through (4) for each droplet results in local values for T_d, u_d, v_d, and D as a function of time. The solution to these equations requires a knowledge of the velocity, temperature and density profiles of the surrounding medium. The properties of the surrounding medium are obtained from the thermal model presented in the next subsection.

Thermal Model for the Surroundings. The second part of the thermal model involves solution of the equations representing the thermal behavior of humid air in a buoyant jet rising above a heated, horizontal disk. The liquid film present on the disk is assumed to evaporate at a constant rate, and the analysis also includes the heat and mass transfer effects that result from either the evaporation from, or condensation on, the water droplets. The possibility of condensation of the warm jet due to the presence of aerosols that are commonly present in the ambient is also considered. The spray considered here is a monodispersed one, and it is assumed to be uniformly distributed throughout the gas phase. For dispersed sprays, the hydrodynamic effects that the spray may have on the gas flow can be neglected. In combustion problems, this phenomena is usually referred to as a one-way coupling problem (Zhou and Yao, 1992). In a similar fashion, a one-way momentum coupling is also used for the condensing aerosol particles due to their extremely low inertia. Other assumptions considered in the gas phase formulation are as follows:

- steady state conditions
- the evaporation rate at the surface of the heater is nearly constant
- the air and water vapor are in thermal equilibrium
- the presence of the droplet generator does not affect the properties of the continuous flow
- viscous dissipation, pressure, and Soret effects are negligible as energy terms
- the Dufour effect is negligible
- the gas flow is laminar, two-dimensional, and axisymmetric

The validity of some of these assumptions is expected to diminish in the vicinity of the heater due to the unpredictable bursting of bubbles arising from the liquid film. Furthermore, a typical heat flux value for spray cooling of the order of 100 $\mathrm{W/cm^2}$ was used to characterize the flow. For this case, the ratio of $\mathrm{Gr/Re}_H^2$ is of order one, which implies that the flow is a buoyant jet and gravity effects should be considered in the analysis throughout the entire domain.

By considering an Eulerian point of view and applying the assumptions, the conservation equations for heat, mass, and momentum transfer of a buoyant jet coupled with a droplet spray and condensing particles are written as follows:

Conservation of Mass.

$$\frac{1}{r}\frac{\partial}{\partial r}(rv) + \frac{\partial}{\partial z}(u) = -\frac{N_{oc}}{\rho}\frac{dm_c}{dt} \tag{10}$$

Conservation of Mass for Water Vapor.

$$\frac{1}{r}\frac{\partial}{\partial r}(rX_A v) + \frac{\partial}{\partial z}(X_A u) = \frac{D_{ab}}{r}\frac{\partial}{\partial r}\left(r\frac{\partial X_A}{\partial r}\right) - \frac{N_{oc}}{\rho}\frac{dm_c}{dt} \tag{11}$$

Conservation of Energy.

$$\frac{1}{r}\frac{\partial}{\partial r}(rvT) + \frac{\partial}{\partial z}(uT) = \frac{\alpha}{r}\frac{\partial}{\partial r}\left(r\frac{\partial T}{\partial r}\right) + \frac{N_{od}}{\rho c_{pm}}(hA_s)_d(T_d - T) - \frac{N_{oc}}{\rho c_{pm}}\left(\frac{dm_c}{dt}h_{fg} - (hA_s)_c(T_c - T)\right) \tag{12}$$

Conservation of Momentum.

$$\frac{1}{r}\frac{\partial}{\partial r}(ruv) + \frac{\partial}{\partial z}(u^2) = \frac{\nu}{r}\frac{\partial}{\partial r}\left(r\frac{\partial u}{\partial r}\right) + gf(X_A, T) \tag{13}$$

Equations (10)–(13) satisfy the conditions at the heated surface and outside of the boundary layer. They must also satisfy symmetry at the center of the jet. Thus, the boundary conditions become

$$u\,(z = 0) = u_o, \quad X_A\,(z = 0) = 1, \quad T\,(z = 0) = T_{\text{sat}},$$

$$v = \frac{\partial u}{\partial r} = \frac{\partial T}{\partial r} = \frac{\partial X_A}{\partial r} = 0 \quad (r = 0),$$

$$u\,(r \to \infty) = 0, \quad T\,(r \to \infty) = T_\infty, \quad X_A\,(r \to \infty) = X_{A,\infty}. \tag{14}$$

High condensation rates on the nucleation particles and high density numbers are expected to maintain the buoyant jet at saturated conditions. A diffusive mass transfer model has been assumed for the condensation that occurs on the nucleation particles. The sensible heat contribution to both the spray and the condensing particles is retained, and the temperature of the condensing particles is assumed to be equal to the local wet bulb temperature.

The function $f(X_A, T)$ in the momentum equation represents both the concentration and the temperature contribution to the buoyancy force. Assuming ideal gas behavior, this function can be expressed for both water vapor and air as (Gebhart et al., 1988)

$$f(X_A, T) = \left[\frac{1 + X_A(M_B/M_A - 1)}{T_\infty/T} - 1\right]. \tag{15}$$

Numerical Solution

The strategy used to solve the set of equations for the droplet spray and the buoyant jet is now discussed. Initially, the presence of the droplets in the buoyant jet are neglected so that two independent solutions can be determined for the conservation equations applied to the buoyant jet and the droplet spray. Once the first solution for the buoyant jet is known, it is used to solve the equations for each droplet, which are given by Eqs. (1) through (4). The energy and mass contribution of the spray into the buoyant jet can be estimated after the first solution for the velocity and temperature distribution of the buoyant jet. This procedure continues until convergence is reached.

The set of nonlinear, ordinary differential equations describing the behavior of a single droplet, given by Eqs. (1) through (4), is solved by using an initial value Runge-Kutta scheme. The second set of nonlinear partial differential equations which describe the conditions in the buoyant jet, Eqs. (10) through (15), is solved by using a finite difference marching scheme in the axial direction. An implicit approach in the radial direction is used to solve the buoyant jet equations. The resulting set of nonlinear buoyant jet equations is solved using Newton-Raphson method for systems of equations in an unique form. Both sets of equations are eventually combined.

Both the single droplet model and the buoyant jet model were independently compared with previously reported analytical solutions and a limited amount of experimental data. The single droplet model predicts temperatures that are within one percent of temperatures obtained from experimental data for a 2.0 mm condensing droplet falling at a constant velocity in a standard ambient, as reported by Kincaid and Longley (1989). The droplet model also predicted the velocity decrease with an error of less than one percent when compared with the analytical solution obtained for a falling solid sphere with a Reynolds number within the Stoke's flow regime. The buoyant jet model was compared with previous solutions for forced laminar jet (Schlichting, 1979), laminar plumes with linear combination of heat and mass transfer effects (Mollendorf and Gebhart, 1974), and laminar free jets with linear buoyancy terms (Himashekar and Jaluria, 1982). In all cases, the thermal model predicted concentrations, temperatures, and velocities that were within two percent of the established limiting solutions, and the solutions were shown to be independent of the grid size for all cases (for details see González et al., 1995).

Numerical Results

Four independent variables were used to characterize the conditions in the jet and the droplets: initial velocity of the vapor, initial droplet diameter, initial droplet velocity, and droplet density numbers. Table 1 shows values for these four variables for the seven cases considered in this paper. Droplet diameters of 75 and 150 μm were considered because they are typical sizes used in spray cooling applications. The model assumes that the droplets are uniformly generated by a variable frequency monodispersed droplet generator based on the Rayleigh break up phenomenon. Droplet frequencies of 0.5 and 1.0 kHz were selected because they correspond to typical generation rates used during the experiments. The selected values of the droplet frequency determine the number of droplets per unit volume, N_{od}, that were generated. The heat flux and the velocity of the water vapor near the heated surface, u_o, are related to each other by assuming that the heat flux at the surface, q''_o, is used to vaporize the liquid, thus

$$u_o = \frac{q''_o}{h_{fg}\rho_v}. \tag{16}$$

This value of u_o was assumed to remain constant. This assumption is valid under nonfluctuating evaporative conditions at the surface. Although steady-state conditions are assumed in this problem, minor fluctuations in the value of q''_o are expected to occur near the heated surface, due to bursting of bubbles in the thin liquid layer of the heater.

Values of 0.75 and 2.5 m/s for u_o, shown in Table 1, correspond to Jet Reynolds numbers of 300 and 900, and heat fluxes of 100 and 300 W/cm^2, respectively. The numerical results are based on a distance between the droplet generator and the heated surface H_o of 100.0 mm and a diameter of the heated surface D_o of 8.0 mm.

Numerical Results For The Saturated Buoyant Jet. Figure 2 shows the nondimensional buoyant jet centerline temperature for Cases 1 through 3 of Table 1. A significant temperature decrease is observed for Case 1 where large diameter and low velocity water droplets were used. Since the spray is introduced

Table 1 Numerical cases considered

Case	u_o (m/s)	u_{di} (m/s)	D_i (μm)	f (kHz)	T_{di} (°C)	T_o (°C)
1	0.75	5	150	1.0	20	100
2	0.75	15	75	1.0	20	100
3	0.75	15	75	0.5	20	100
4	0.75	10	150	1.0	20	100
5	2.50	5	150	1.0	20	100
6	2.50	5	150	1.0	20	100
7	2.50	18	75	1.0	20	100

into the jet at $Z = 1$ where the temperature is lower than the local jet temperature, the jet experiences a significant cooling for the case of large droplets. For droplets with low velocities, the cooling effect on the jet will be larger due to longer droplet residence times.

Comparison of Cases 2 and 3 shows the effect of the droplet number density, given by the droplet frequency generation rate, on the temperature of a saturated jet. The temperature decrease is larger for large droplet densities (Case 2) than for small droplet densities (Case 3). At intermediate Z values, the jet temperature is higher for cases where the spray is present, due to the fact that at these locations the droplets have reached thermal equilibrium such that their temperature is equal to the local wet bulb temperature of the jet. The wet bulb temperature will be higher than the actual local jet temperature when supersaturation values are present, giving rise to regions where the presence of the drops will actually heat the jet. The jet temperature shows significant changes for all three spray cases considered (Case 1, 2, and 3) when compared with the non-spray solution. Trends in the numerical results for the dimensionless buoyant jet centerline concentration and dimensionless velocity are similar to those obtained for the dimensionless temperature.

Numerical Results For The Spray. Results for the droplet axial velocity, diameter, and temperature for 150 μm droplets that are injected along the jet centerline are shown in Figs. 3 through 5. Droplet initial velocities of 5 and 10 m/s, and jet velocities of 0.75 and 2.5 m/s were considered (see Table 1). From Fig. 3, it can be seen that at small values of Z_d (for the droplet, $Z_d = 0$ is the location of the droplet generator, and $Z_d = 1$ is the location of the heated surface) the droplets experience acceleration. The acceleration is a result of an increase in the droplet mass as condensation occurs on the drop when it is first introduced into the moist jet. The droplet diameter plotted in Fig. 5 shows the increase in droplet size that occurs as long as the droplet has a temperature lower than the local wet bulb temperature of the jet. Once the droplet has reached a maximum diameter, it starts to decelerate. Figure 3 also shows that the velocity decrease is highly affected by the jet velocity, as indicated by the slope of the droplet velocity curves. For higher jet velocities, the droplet experiences larger drag forces resulting in a significant reduction in velocity.

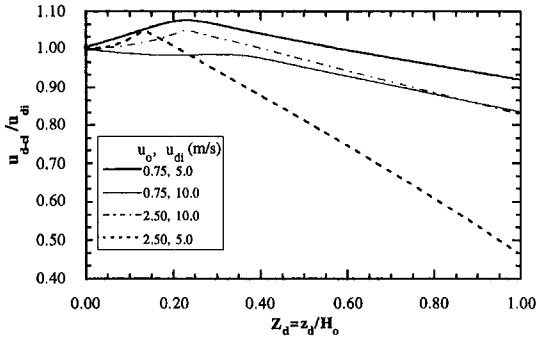

Fig. 3 150 μm droplet velocity at $R = 0$ (centerline)

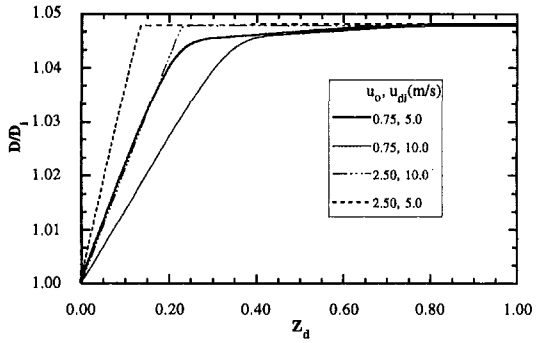

Fig. 4 150 μm droplet diameter at $R = 0$ (centerline)

Condensation stops once the droplet temperature reaches the local wet-bulb temperature in the jet, as seen in Fig. 5. This figure shows that droplets with higher initial velocities reach the wet bulb temperature later than those with lower initial velocities. This figure also shows that the droplets do not experience further heat transfer after they have reached saturation conditions. Figure 5 indicates that the diameter of a rapidly moving droplet in a jet with low velocity increases slower than the diameter of a slowly moving droplet in a high velocity jet.

The radial velocity variation along the axial direction for the case of a 150 μm droplet was also investigated. Results showed that the influence of entrainment and initial droplet momentum dominate the radial momentum balance and that Saffman forces play a small role and do not affect the radial velocity. It was also shown that the maximum radial velocity of the droplets were less than one percent of the minimum axial velocity. This result suggests that for the cases considered here, the droplets do not deviate significantly from their initial, vertical projected path and once they are injected vertically into the jet, they will reach the heated surface.

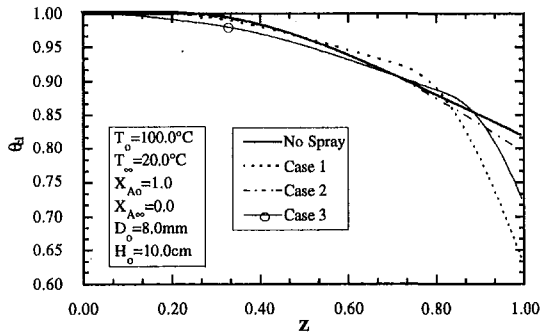

Fig. 2 Saturated jet centerline temperature

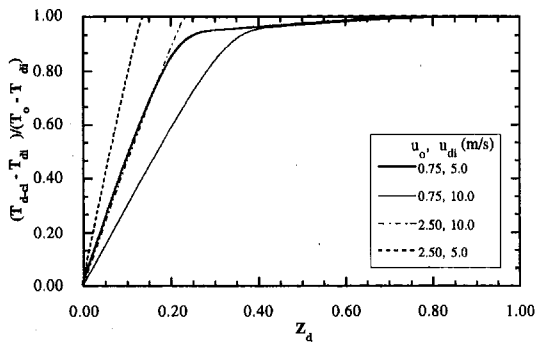

Fig. 5 150 μm droplet temperature at $R = 0$ (centerline)

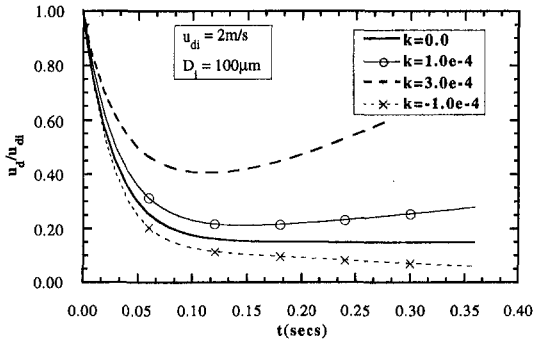

Fig. 6 Condensation/evaporation effects on droplet velocities

Discussion Of Numerical Results. Droplet diameters of 75 and 150 μm at different initial velocities along with jet velocities of 0.75 and 2.5 m/s were considered. These droplet diameters and jet velocities represent typical spray and surface heat fluxes that are encountered in spray cooling applications. A strong dependence between the jet and the spray conditions was shown to exist; that is, the thermal behavior of the jet is highly affected by the spray conditions, while the spray properties are strongly influenced by the initial conditions of the jet.

In most of the cases presented, condensation occurred on the droplets as they approach the heated surface, resulting in initial acceleration until they reach their maximum diameter. The effects of condensation on the velocity of the droplet can be shown by expanding Eq. (1) for a single droplet with constant temperature falling in a quiescent ambient and considering the vapor in the jet moving in the direction opposite to that of the droplet. For this case, Eq. (1) becomes

$$\frac{du_d}{dt} = g + \frac{3u_d}{D}\left[\frac{dD}{dt} - \left(\frac{3}{4}\right)\left(\frac{\rho_m}{\rho_l}\right)C_d u_d\right]. \qquad (17)$$

Equation (17) indicates that acceleration of the drops occurs when the increase in the weight caused by condensation is larger than the opposing drag force. Also note that for evaporating droplets, deceleration will always occur. Equation (17) was solved for the simple linear case in which the evaporation/condensation rate is equal to a constant, or $D = D_i + kt$ (k in m/s), and for low initial droplet velocity so that the Reynolds number was within the Stoke's flow regime. Results of this solution are shown in Fig. 6. The figure shows that an evaporating, or a solid droplet, experience deceleration, i.e., k values less or equal to zero, while a condensing one (positive k values) experience acceleration.

Numerical results show that the thermal behavior of the droplets close to the external region of the boundary layer are less affected than those close to the jet centerline. However, those droplets at the edge of the jet experience jet entrainment effects that tend to drag the droplets toward the centerline. Even though low droplet velocities were considered, in all cases the droplets reached the heated surface for the 100 mm travel distance that was considered in this study. For the case of either larger travel distances or smaller droplets, this might not be the case because these conditions will encourage the migration of the droplets away from the heated surface.

Finally, the numerical results presented in this section show that the droplets reach the plate at fully saturated conditions. The low thermal mass of the droplets considered causes the droplets' temperature to rapidly reach the wet bulb temperature of the saturated jet. Therefore, saturation conditions should be expected for small droplet sprays prior to impact on the heated surface. This interesting result might be an explanation for previous reports by Bonacina et al. (1979) and Toda (1974) where negligible subcooling effects in spray cooling applications were experienced when using small droplet sprays.

Experimental Set-Up

The objective of the experiment was to validate the mathematical formulation for the thermal and hydrodynamic behavior of droplets falling in both a constant and variable-property ambient. The apparatus used during the experiments consisted of a droplet generator, photographic equipment, and a heated surface. A schematic of the experimental set-up is shown in Fig. 7. Water droplets were generated by using the theory of instability of capillary jets first reported by Rayleigh (1878). This theory suggests that a continuous jet of diameter d_j and velocity u_j can be broken into uniform droplets if the jet is disturbed by an optimum frequency f. The liquid must exceed a minimum velocity to form a liquid jet.

A modified ink-jet printer head was used as a droplet generator during the experiments. The printer head had a rectangular plate with 32 orifices and each orifice had a diameter of 50 μm. All orifices were separated by a distance of 1.5 mm. Behind each orifice was a piezoelectric crystal which was driven by a frequency generator as shown in Fig. 7. Frequencies between 100 Hz and 15 kHz were used.

Droplets were generated by activating the piezoelectric crystals at several frequencies causing a disturbance in the continuous jet. The initial diameter of the liquid droplets was calculated from the knowledge of the jet velocity and the optimum disturbance frequency by applying the conservation of mass between the fluid leaving the orifice and an adjacent position after the droplets had been formed. This process yields an expression for the droplet diameter of

$$D = \left(\frac{3}{2} d_j^2 \frac{u_j}{f}\right)^{1/3}. \qquad (18)$$

Several droplet diameters between 125 and 200 μm were generated by varying the liquid pressure and the frequency of the piezoelectric crystals.

The photographic equipment used during the experiments consisted of a microscope with variable magnification and a variable frequency stroboscopic light. The combination of the microscope with the stroboscopic light allowed observation of the magnified stationary droplets. The microscope was attached to a video camera and images of the droplets were stored on a video cassette. The images of the droplets could also be simultaneously observed on a video monitor. The magnification of the photographic system was determined by taking a photograph of a reference scale before and after each test. The uncertainty in the measurements of the droplet diameters was less than two percent, considering the error involved in the magnification.

The heated surface consisted of a large diameter copper cylinder that was tapered to a small horizontal circular area with a diameter of 8.00 mm at the tip. The copper cylinder had a total length of 85 mm. The bottom section of the cylinder was 58 mm high and had a 38 mm diameter. The diameter of the bottom section was reduced to 8.00 mm, forming a cone with length of 14 mm (see Fig. 7).

The energy input to the copper cylinder was provided by a 450 Watt, 240 Volt electrical heater attached to the 38 mm diameter base. The copper cylinder was well insulated to minimize heat losses from the side and bottom surfaces. Heat flux measurements from the cylinder were provided by nine type-K thermocouples placed close to the tip of the copper surface, as shown in Fig. 7. Each axial layer of thermocouples was separated vertically by 3.2 mm, and each of the three thermocouples was equally spaced around the circumference of the top of the copper cylinder. The vertical distance between the surface of the cylinder and the closest set of thermocouples was 6.4 mm. The heat flux was calculated by assuming one-dimensional conduction along the axial direction of the cylinder at the location of the thermocouples. An uncertainty analysis was performed considering errors in thermocouples and distances between them

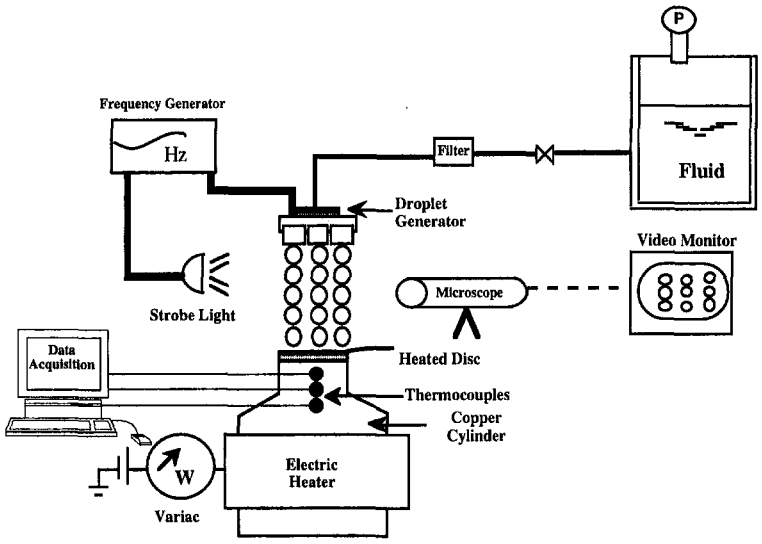

Fig. 7 Experimental apparatus

which resulted in an overall error in the calculated heat flux of less than ten percent. The one-dimensional assumption was verified by estimating heat losses from the heater to the ambient and performing an energy balance under steady-state conditions. This one-dimensional assumption resulted in an error of less than five percent.

Experimental Results

The variables investigated in the experiments included droplet diameters and velocities, as functions of the vertical direction. Two basic experiments were considered: the study of a single stream of water droplets in a constant property ambient, and the study of a stream of water droplets prior to impact on a horizontal heated disc which has an evaporating liquid water film on the surface.

Experiments Without Buoyant Jet. Droplet velocities and diameters were measured at various frequencies when the droplets were injected into a constant property, stagnant ambient air (no heater present). The absence of the heater allowed the study of a stream of droplets at room conditions. Two fluid pressures, 9 kPa and 19 kPa, were chosen.

Photographs of the droplets were taken at several vertical distances by fixing the location of the microscope and varying the height of the droplet generator. Droplet diameters were obtained by photographing the droplets and then a calibrated scale. Velocities were obtained by measuring the distance between droplets at various distances from the print head. The droplet velocity was then calculated from the expression

$$u_j = Lf/M \tag{19}$$

where L is the distance between droplets measured from the photographs, f is the droplet generation frequency, and M is the photographic magnification. The estimated error in predicting droplet velocity from Eq. (19) is within four percent. Photographs were taken up to a vertical position where the monodispersity was lost due to the coalescence of the droplets. This maximum distance varied between 60 and 100 mm. Precautions were taken to avoid air currents in the room. An example of the measured droplet velocity is shown in Fig. 8. Comparison with velocities predicted with the droplet model is also shown for the figure.

By varying the frequency at which the droplets were generated, the drag model used to determine droplet interference effects could be verified. Different values of the critical distance for which adjacent drops influence the drag coefficient, $(L/D)_{crit}$, were used in the droplet hydrodynamic model. For values of L/D greater than the critical value, the drag coefficient was based on a single droplet. For values of L/D less than the critical value, the drag coefficient must be modified to account for the influence of adjacent droplet. The value of $(L/D)_{crit}$ has not been clearly established in the literature. However, Mullholland (1988) suggests a value between four and ten. The results in Fig. 8 are based upon a value of $(L/D)_{crit}$ equal to ten. This value appears to provide the best correlation between the experimental velocity measurements and the velocity values predicted by the hydrodynamic model, with an accuracy within ten percent for all test conditions.

The temperature and relative humidity of the room averaged 25.0°C and 40 percent, respectively, during the tests. For these conditions, the diameter of the droplet was expected to decrease slightly as a result of evaporation to the ambient air. However, the short distances of travel that the droplet experienced caused small variations in droplet diameter, and decreases of less than ten percent were observed. The measured droplet diameters compared within five percent with the value predicted by Eq. (18).

Experiments With Buoyant Jet. The objective of these experiments was to verify the coupled model of droplet sprays prior to impact on a surface that is heated above the saturation temperature of the liquid spray. Spray conditions were fixed at a droplet frequency of 10 kHz, a liquid pressure of 19 kPa, initial droplet temperature of 25°C, and droplet generator height

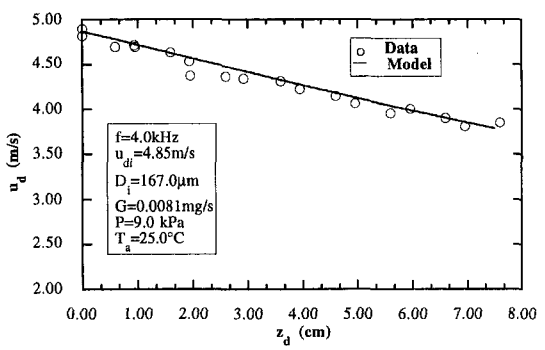

Fig. 8 Comparison of measured and calculated values of droplet velocities

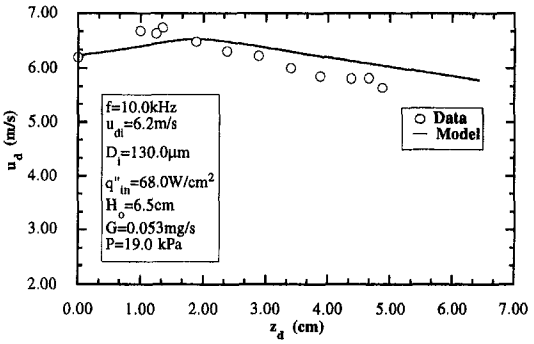

Fig. 9 Experimental and numerical values of the velocity of a stream of droplets in a buoyant jet

above the heated surface, H_o, of 65 mm. This particular set of spray conditions resulted in an average droplet diameter of 130 μm. All heater conditions were fixed at a steady-state heat flux and surface temperature of 68 W/cm^2 and 115°C, respectively. These spray and heater conditions are similar to conditions achieved from commercial nozzles reported by Bonacina et al. (1979). In their case, surface heat fluxes close to 100 W/cm^2 were reported for surface temperatures of 112°C, subcooling of 75°C, and droplet average diameters less than 100 μm.

Five streams of droplets were used to uniformly cover the entire 8.0 mm-diameter heated surface. The distance between the orifices was 1.5 mm. Therefore, the pattern from five orifices provided a fairly uniform coverage on the heated surface. Photographs of the streams of droplets were taken at different vertical distances above the heated surface by fixing the droplet generator at a distance H_o of 65 mm and moving the microscope in the vertical direction. The procedure to measure velocities and diameters was similar to those of the constant ambient experiments. However, for the ambient with variable properties, a lower magnification, on the order of 20 ×, was used because it was extremely difficult to position the microscope close to the heater due to condensation on the microscope lens. Also, data close to the droplet generator exit was difficult to observe with the microscope and the velocity was estimated from a hydrostatic balance.

The data for the droplet velocities in all the experiments were consistently within ten percent for a given vertical location, indicating good repeatability. The heated surface was observed to be fully covered by an evaporating liquid film during most of the tests. However, minor changes in the wetted pattern affected the distribution of the water vapor within the buoyant jet.

A comparison of the droplet velocities predicted by the numerical model and the measured droplet velocities is shown in Fig. 9. The numerical calculations were obtained by solving the conservation equations for the combined spray and saturated buoyant jet models and using input variables shown in the title box of Fig. 9. The agreement between model and experimental data was within 15 percent. However, the deceleration trend predicted by the theoretical model is slightly different from the one indicated by the measured data. The disagreement is mainly due to the assumptions used in the buoyant jet model, namely, negligible presence of the droplet generator and constant vapor velocity at the heater surface. These assumptions are not completely valid for the small distance of 65 mm between the droplet generator and the heated surface. For larger distances, the effects of variations in the vapor velocity due to bursting bubbles are expected to diminish under steady-state boiling conditions. Furthermore, the model assumption of uniform droplet distribution may have affected the results. In the experiments performed, the heated surface was covered by a line of five droplet streams instead of being exactly distributed uniformly across the surface. However, the model does predict the general trend of the condensation and the acceleration followed by deceleration that exists when multiple droplets travel through a saturated medium.

Conclusions

This research reports a comprehensive investigation of the behavior of small droplet sprays that were initially subcooled and downward oriented prior to their impact on a horizontal heated surface. This situation commonly arises in spray cooling applications. An experimental and theoretical investigation of the coupled effects between a downward oriented spray and a rising saturated buoyant jet, which results from a constant evaporation on a heated surface, are reported. A model describing the thermal and hydrodynamic behavior of both the spray and the saturated buoyant jet is developed. A two-dimensional Lagrangian formulation is used to describe the conditions of the spray while the temperature and velocity distribution in the buoyant jet is described by an Eulerian formulation in cylindrical coordinates. An experimental set-up involving a high speed photographic apparatus was used to observe vertically projected monodispersed sprays and measure the diameter and velocity of the droplets as they approached the horizontal heated surface. The theoretical formulation was calibrated against several established theoretical limiting cases and reported data. The full theoretical model was also compared with data gathered in this research; numerical results were within 15 percent of the experimental values. Further theoretical and experimental results indicate that:

- The temperature of the saturated buoyant jet is influenced by the presence of a liquid spray that is initially subcooled.
- The saturated jet experiences high supersaturation levels due to the absence of sufficient condensation nuclei that are needed to maintain saturated thermal equilibrium.
- Vertically projected small droplet sprays in spray cooling applications experience high condensation rates while in contact with a saturated buoyant jet and reach the saturation temperature before impacting the heated surface, thus inhibiting any sub-cooling effects. These droplets may also experience acceleration as a consequence of an increase in mass due to condensation that can occur on the drops.
- The presence of the saturated buoyant jet increases the drag forces on the spray resulting in considerable reduction in droplet velocities. Droplets close to the edge of the jet free boundary experience a "trapping" effect that forces them toward the centerline, as dry ambient fluid is entrained in the jet.
- Closely spaced droplets experience smaller drag coefficients than exist for widely spaced drops.

Finally, this research approach establishes the basis for a unified theory for spray cooling that includes pre-impact and post-impact processes. A unified theory will enable designers to specify spray parameters which will lead to the control of high heat transfer rates in practical applications. The unified spray cooling theory should be a topic of further discussion among researchers.

References

Bacon, F. M., Cowgill, D. F., Hickox, C. E., Walko, R. J., Subia, S. R., and Riedel, A. A., 1984, "High Heat Flux Target for Intense Neutron Source," *Review of Scientific Instruments,* Vol. 55, pp. 42–47.

Bonacina, C., Del Giudice, S., and Comini, G., 1979, "Dropwise Evaporation," ASME JOURNAL OF HEAT TRANSFER, Vol. 101, pp. 441–446.

Choi, K. J., and Yao, S. C., 1987, "Mechanisms of Film Boiling Heat Transfer of Normally Impacting Spray," *International Journal of Heat and Mass Transfer,* Vol. 30, pp. 311–318.

Deb, S., and Yao, S. C., 1989, "Analysis on Film Boiling Heat Transfer of Impacting Sprays," *International Journal of Heat and Mass Transfer,* Vol. 32, pp. 2099–2112.

Fuchs, N. A., 1964, THE MECHANICS OF AEROSOLS, Pergamon Press, New York.

Gebhart, B., Jaluria, Y., Mahajan, R. L., and Sammakia, B., 1988, BUOYANCY INDUCED FLOWS AND TRANSPORT, Hemisphere, New York.

Ghodbane, M., and Hollman, J. P., 1991, "Experimental Study of Spray Cooling with Freon-113," *International Journal of Heat and Mass Transfer,* Vol. 34, pp. 1163–1174.

González, J. E., Black, W. Z., and Desai, P. V., 1995, "Numerical Solution of Saturated Laminar Buoyant Jets," *Proceedings of the ASME Heat Transfer Division,* Vol. 317–1, pp. 321–329.

Gu, C. B., Su, G. S., Chow, L. C., and Pais, M. R., 1993, "Comparison of Spray and Jet Impingement Cooling," ASME Paper 93-HT-20.

Hall, D. D., and Mudawar, I., 1995, "Experimental and Numerical Study of Quenching Complex-Shaped Metallic Alloys with Multiple, Overlapping Sprays," *International Journal of Heat and Mass Transfer,* Vol. 38, pp. 1201–1216.

Himashekar, K., and Jaluria, Y., 1982, "Laminar Buoyancy-Induced Axisymmetric Free Flows in a Thermally Stratified Medium," *International Journal of Heat and Mass Transfer,* Vol. 25, pp. 213–221.

Kincaid, D. C., and Longley, T. S., 1989, "A Water Droplet Evaporation and Temperature Model," *Transaction of the ASAE,* Vol. 32, pp. 457–460.

Liu, Z., and Reitz, R. D., 1995, "Modeling Fuel Spray Impingement and Heat Transfer Between Spray and Wall in Direct Injection Diesel Engines," *Numerical Heat Transfer-Part A: Applications,* Vol. 28, pp. 515–529.

Mollendorf, J. C., and Gebhart, B., 1974, "Axisymmetric Natural Convection Flows Resulting From the Combined Buoyancy Effects of Thermal and Mass Diffusion," *Proceedings of the 5th, International Heat Transfer Conference,* Tokyo, pp. 10–14.

Mullholland, J. A., 1988, "Influence of Droplet Spacing on Drag Coefficient in Nonevaporating, Monodisperse Streams," *AIAA Journal,* Vol. 26, pp. 1231–1237.

Ohkubo, H., and Nishio, S., 1987, "Mist Cooling for Thermal Tempering of Glass," *Proceedings of the ASME-JSME Thermal Engineering Joint Conference,* Vol. 5, pp. 71–78.

Pedersen, C. O., 1970, "An Experimental Study of the Dynamic Behavior and Heat Transfer Characteristics of Water Droplets Impinging Upon a Heated Surface," *International Journal of Heat and Mass Transfer,* Vol. 13, pp. 369–381.

Poo, J. Y., and Ashgriz, N., 1991, "Variation of Drag Coefficients in an Interacting Drop Stream," *Experiments in Fluids,* Vol. 11, pp. 1–8.

Rayleigh, L., 1878, "On the Instability of Jets," *Proceedings of the London Mathematical Society,* Vol. 10, pp. 4–13.

Saffman, P. G., 1965, "The Lift of a Small Sphere in a Slow Shear Flow," *Journal of Fluids Mechanics,* Vol. 22, pp. 385–400.

Saffman, P. G., 1968, "Corrigendum," *Journal of Fluids Mechanics,* Vol. 31, p. 624.

Schlichting, H., 1979, BOUNDARY LAYER THEORY, Seventh Ed., McGraw-Hill, New York, pp. 230–234.

Toda, S., 1974, "A Study of Mist Cooling (2nd Report: Theory of Mist Cooling and Its Fundamental Experiments)," *Heat Transfer: Japanese Research,* Vol. 3, pp. 1–44.

Watson, R. D., 1990, "Structures for Handling High Heat Fluxes," *Journal of Nuclear Materials,* Vol. 176 & 177, pp. 110–121.

Yuen, M. C., and Chen, L. W., 1976, "On Drag of Evaporating Liquid Droplets," *Combustion Science and Publication,* Vol. 14, pp. 146–154.

Zhou, L., 1993, THEORY AND NUMERICAL MODELING OF TURBULENT GAS-PARTICLE FLOWS AND COMBUSTION, CRC Press, Inc., Florida.

Zhou, Q., and Yao, S. C., 1992, "Group Modeling of Impacting Spray Dynamics," *International Journal of Heat and Mass Transfer,* Vol. 35, pp. 121–129.